Dynamic Light Scattering with multiple 2D Detectors

Anton Fetzer, Ulm University, Germany

FS-CXS Group at DESY

September 5, 2018

Abstract

Summer Student report on the investigation of dynamic light scattering of colloidal solutions using multiple 2D Detectors, as part of the DESY Summer Student Programme 2018. A set of cameras is used as 2D detectors, to record the speckle pattern of a laser beam, diffracted by particles in colloidal solutions to demonstrate the feasibility of observing the decorrelation of the speckle pattern at several Q-values simultaneously.

Contents

1 Introduction

The the advent of the laser, as a practicable source for coherent light, enabled a wide range of applications, including many investigative methods, like Dynamic Light Scattering (DLS) [1]. To perform DLS, one simply shines a coherent light beam on a sample, which contains moving or changing scattering centres. Without the need for any further optics, one can observe the scattered light at a detection plane and determine from it a multitude of properties about the sample, which are usually not directly observable. Advances in detector and computational technologies and the recent availability of coherent light with ever smaller wavelengths at modern synchrotron and free electron laser facilities to observe scattering on ever smaller length scales, show the necessity to revisit the basics of DLS, both for training purposes and the verification of experimental and analysis techniques. This report documents an attempt to do this in the scope of the 2018 Summer Student Programme at DESY using multiple 2D image sensors as detectors for dynamic scattering patterns of optical laser light, scattered from nano particles.

2 Theory

2.1 Scattering

When a plane wave with incident wave vector $\vec{k_i}$ scatters elastically on an massive scattering center, the wavelength of the outgoing wave can be assumed to be unaffected by the scattering, thus $|\vec{k_i}| = |\vec{k_s}|$ with $\vec{k_s}$ being the vector of the outgoing wave. The scattering vector $\vec{Q} = \vec{k_i} - \vec{k_s}$ denotes the difference between the in- and outgoing wave vectors and can be used as a parameter to compare scattering events.
The absolute value of $\vec{q}$ is given by

$$Q = \frac{4\pi n \sin(\theta)}{\lambda} \tag{1}$$

in a medium of refraction coefficient n, with the scattering angle θ and the wavelength λ of the electromagnetic wave. [1, p. 25f]

If coherent light is scattered from a disordered system of many scattering centers, then the scattered light will interfere and form a disordered 'speckle' interference pattern at the detection plane.

2.2 Diffusion

If the scattering centers move according to a specific dynamic, then a corresponding dynamic in the speckle pattern can be observed. [2, p. 1]

The dynamics of spherical microscopic particles in a colloid solution is given by the Stokes-Einstein relation, which specifies the diffusion coefficient D

$$D = \frac{k_B T}{6\pi\eta R} \tag{2}$$

in terms of temperature T, Boltzmann constant k_B, viscosity η of the medium and the radius R of the particles. [4, p. 555]

2.3 Autocorrelation

The instantaneous intensity $I(t)$ scattered off a colloid solution of nano particles and recorded by a point detector, changes erratically due to the diffusion of the particles.

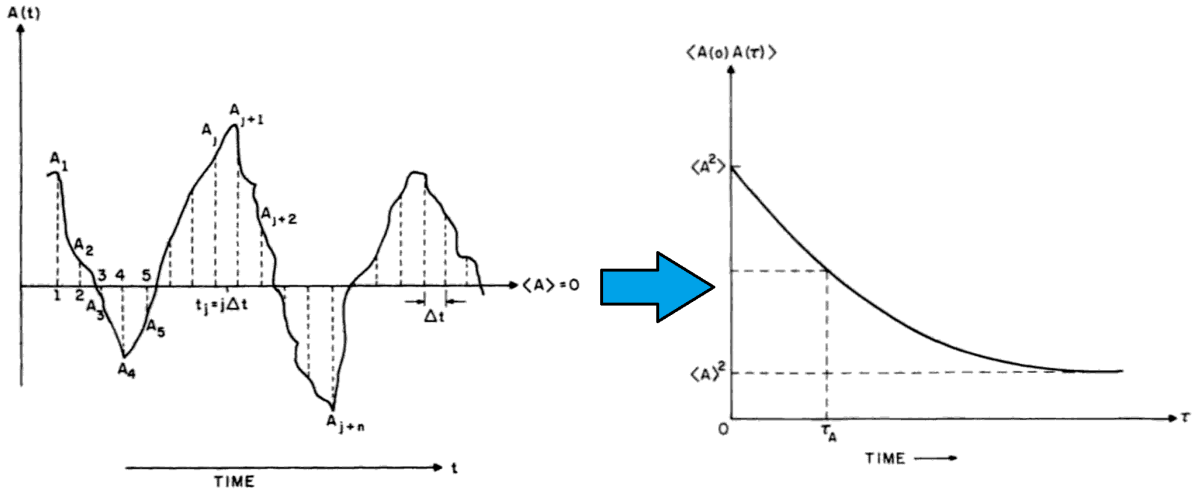

Figure 1: Exemplary plot of an erratically fluctuating property $A(t)$ with corresponding autocorrelation function $\langle A(t)A(t+\tau)\rangle_t$ [1, p. 12f]

As shown in figure 1, the underlying dynamics of such fluctuating properties becomes more apparent, if its autocorrelation function is calculated.

The normalised autocorrelation function of $I(t)$ is refereed to as $g_2(\tau)$ with

$$g_2(\tau) = \frac{\langle I(t)I(t+\tau)\rangle}{\langle I(t)\rangle^2} \tag{3}$$

$g_2(\tau)$ shows, how well correlated pairs of intensities $I(t)$, with a given time difference τ, are on average. Because the signal changes with a finite rate, $g_2(\tau)$ starts at a global maximum and decays with increasing τ, if the signal is not periodic.

In the case of disperse spherical particles undergoing Brownian motion, $g_2(\tau)$ can be shown to follow the relation

$$g_2(\tau) = 1 + \beta^2 \exp(-2DQ^2\tau) \tag{4}$$

with the factor β^2 accounting for the contrast of the speckle pattern, the diffusion coefficient D and the scattering wave vector Q as introduced above.[2, p. 6]

The product $DQ^2 = \frac{1}{t_0}$ is the inverse of the relaxation time t_0 of the system.

2.4 Contrast

The $g_2(\tau)$ does not have to be determined using individual point detectors. If data from a pixel array is avaliable, then $g_2(\tau)$ can be computed from the contrast function c_2, as shown in reference [3, p. 3f].
The contrast function c_2 is the normalised variance of the pixel intensities $I_i(t)I_i(t+\tau)$ in images with pixel index i, added with varying time difference τ and averaged over t, analogous to the autocorrelation function.

$$c_2(\tau) = \left\langle \frac{\sigma(I_i(t) + I_i(t+\tau))_i^2}{\langle I_i(t) + I_i(t+\tau)\rangle_i^2} \right\rangle_t \tag{5}$$

g_2 is then simply given from c_2 and the average single image contrast β^2 [3, p. 3f]

$$g_2(\tau) = 2 \cdot c_2(\tau) - \beta^2 + 1 \tag{6}$$

3 Experiment

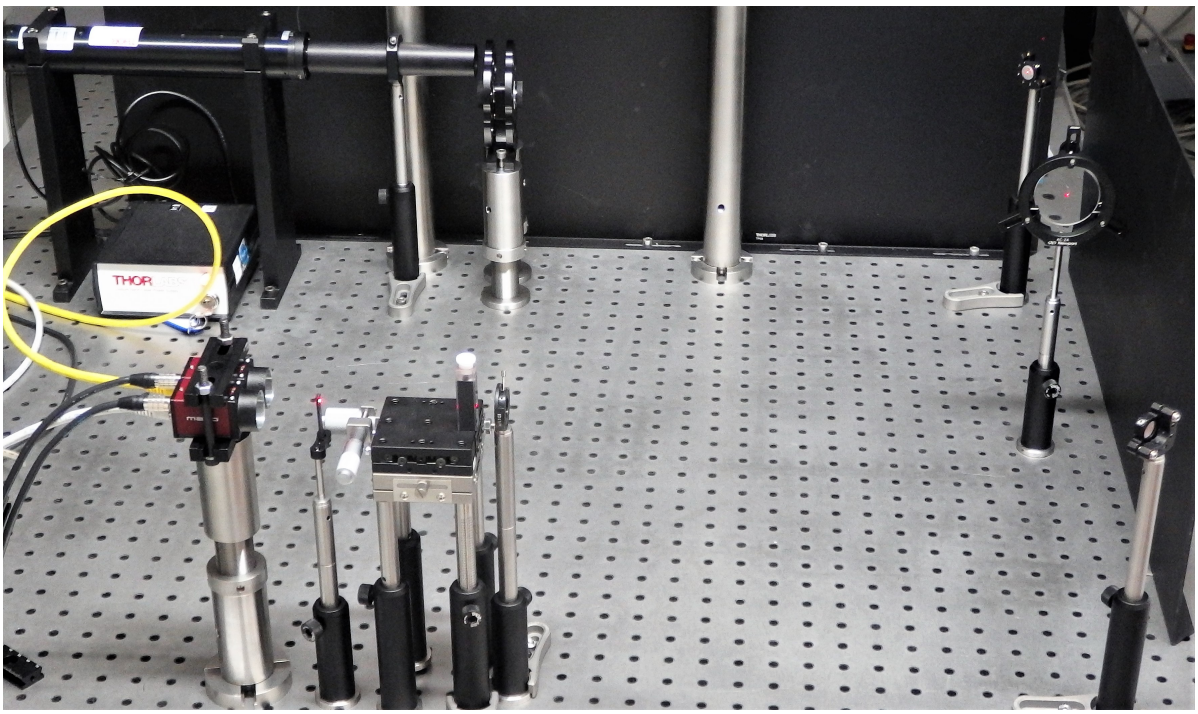

Figure 2: Photo of the final setup with the laser in the back, two mirrors, a lens with very long focal length, the iris in front of the sample cuvette on the sample stage, the beam stop and the two symmetrically mounted cameras.

The used setup shown in figure 2 and sketched in 3 consists of the HeNe laser, specified in table 1 and the cameras specified in table 2, as well as two plain mirrors, a lens

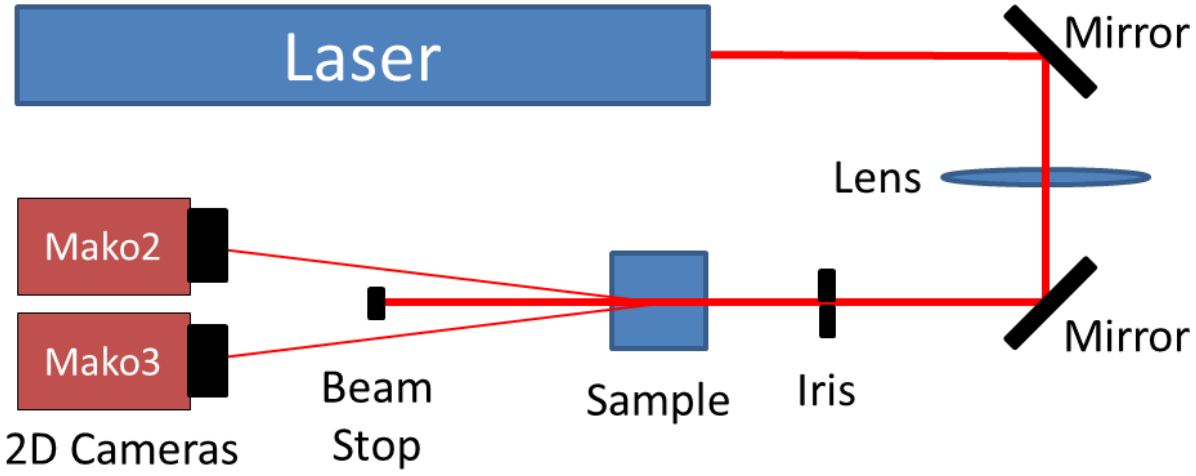

Figure 3: Sketch of the final setup as seen in figure 2 with the laser in the back, two mirrors, a lens with very long focal length, the iris in front of the sample cuvette on the sample stage, the beam stop and the two symmetrically mounted cameras.

with more than 1m focal length, the sample in a shielded cuvette, a black cardboard beam stop and a sample stage. The long distance between laser and sample, as well as the iris are meant to improve the beam quality, while the lens reduces the beam diameter to fit into the sample cuvette, without causing scattering on the edges of the cuvette.

Table 1: Characterisation of the used HeNe laser HNL020R from Thorlabs

Parameter	HeNe Laser
Wavelength	632.8 nm
Power	2 mW
Beam Diameter	0.63 mm
Beam Divergence	1.3 mrad
Polarisation	Random

For the first measurements only one camera of type Thorlabs DCC1545M was used, to see, if the setup was working at all, with the Mako G-125 cameras added later, once the functionality was confirmed. All data shown in this report, was obtained using the Mako G-125 cameras.

The two cameras are connected to the same external trigger and were used to record images synchronously.

During the course of the project, several different samples were used, but most of the usable data was collected using samples, taken from the same flask of Polybead 200nm microspheres from Polysciences Inc. This report will therefore only focus on

Table 2: Characterisation of the used Mako G-125 cameras from Allied Vision

Parameter	Mako G-125
Resolution	1292 (H) x 964 (V)
Sensor	Sony ICX445
Sensor type	CCD Progressive
Pixel size	3.75 µm x 3.75 µm
frame rate	30.3 fps

these samples.

4 Analysis

The images recorded by the cameras were saved with the TangoVimba control software in .mbin raw binary file format for easy processing with Matlab and because of the time stamp with microsecond precision in the file header.

The Matlab script "mbinReadIn.m" was used to read in the separate image files and to condense the data into one file. First the directory of the data has to be specified, in which a sub-folder containing the .mbin files is located, with the name of the sub folder being the name of the camera. The script reads the relevant parameters of the images from the header of the first file and extracts the pixel data from all images in sequential order, together with the corresponding time stamps. The time stamp of the first file is subtracted from all the following files, to get the relative time since the first image.

The read-in script also creates an animated .gif file of the data in the subdirectory, to provide a convenient visualisation.

An optional dark image subtraction routine was also implemented, but rarely used, due to the good signal to noise ratio of the measurements.

The images are split into a number of equally sized vertical stripes, if a stripe number more than one was specified in the variable "numStripes" at the top of the script.

In the last step, all saturated pixels with pixel values greater than 254 are excluded from the dataset, before the matrix "IMS" containing all pixels from all images and stripes and the time vector are stored together in a .mat file.

This .mat file can be accessed by the script "mbinAnalysis" in which the actual analysis of the data is done. At the top of the script, one can specify under which angle, from the forward direction, the measurement was done, as well as how much of the data is used for the actual calculations, which can have a significant impact on the time needed for the calculations.

To calculate the c_2 function, two images at a time, with all possible combinations of time differences are added together, before the contrast of the stacked images is calculated according to formula 5.

Next, the single image contrast β is calculated by dividing the standard deviation of the pixels in each image, by their mean.

The function $g_2 - 1$ is calculated according to formula 6 and fitted with the function

$$g_{2fit} = a \cdot \exp(-2 \cdot \tau / t_0) + c \tag{7}$$

where a accounts for the contrast and c for an eventual offset of the data, while t_0 is the relaxation time of the system, which can be used to calculate the radius of the scattering centers according to equations 1 and 2

The rest of the script deals with the visualisation of the results by plotting the c_2 functions, the g_2 functions with corresponding fitted curves and a summary of the fit parameters depending on the stripe number and therefore scattering angle, as well as the evolution of the single image contrast over the dataset.

5 Results

5.1 Data Quality

The analysis of the first measurements showed, that the signal quality depends on a multitude of factors. The concentration of the particles needs to be just high enough to avoid multiple scattering, but high enough, to provide a steady signal. Scattering from parts of the experimental setup, like the cuvette or the iris, can also strongly effect the measurement. Having to many saturated pixel in the data, also causes artefacts in the calculated c_2 and g_2 functions.

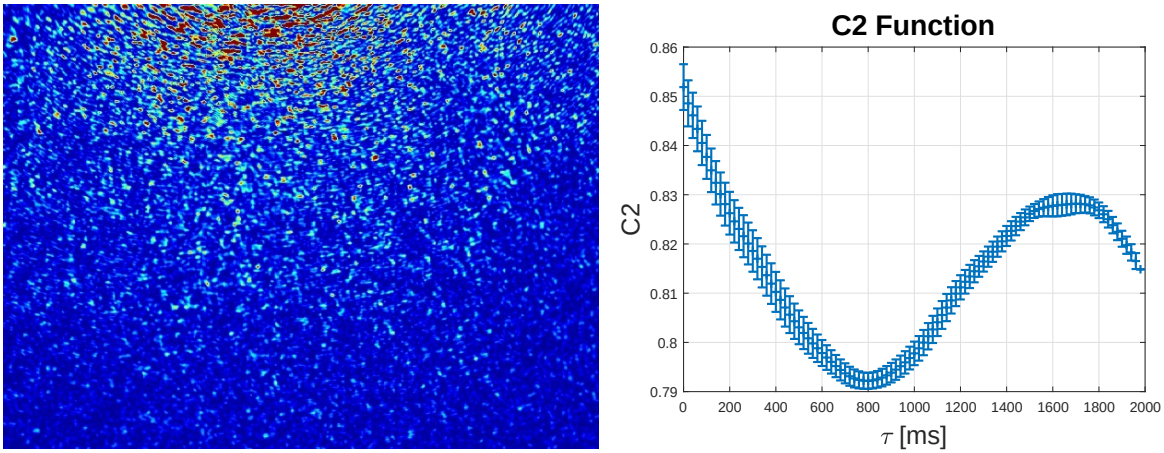

(a) One colour coded frame of a measurement with the beam just above the sensor.

(b) Calculated c_2 function of the same measurement.

Figure 4

In figure 4 such a measurement is shown, where the particle concentration was too low and the forward beam to close to the camera.

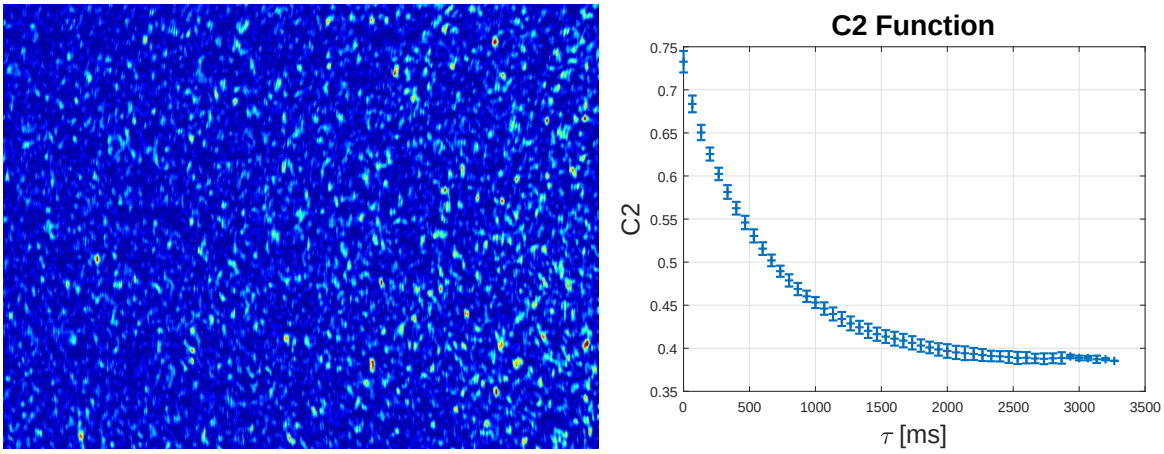

(a) One colour coded frame of a relatively artefact free measurement.

(b) Calculated c_2 function of the measurement on the left, which shows no visible artefacts.

Figure 5

The measurement in 5 shows a relatively artefact free image with a smooth exponentially decaying c_2 function.

5.2 G2 Functions

The fitting of the calculated g_2 functions provides the relaxation time t_0, which can be used according to equation 4 to calculate the radius of the particles. Even though some of the g_2 functions follow the predicted exponentially decaying behaviour very nicely, the relaxation times obtained from the fits did not agree with the theory. The actual particle radius was determined to be 110 ± 10 nm from measurements using a commercial DLS setup.

In figure 6 the g_2 functions from a simultaneous symmetric measurement with both camera sensors at an angle of 7.5° from the forward beam. The scattering angle θ is therefore 3.75°. Using this angle, the determined radius of the particles approximately 400 nm and therefore almost four times larger than the expected value. Further investigations have to be performed to determine the cause of this discrepancy.

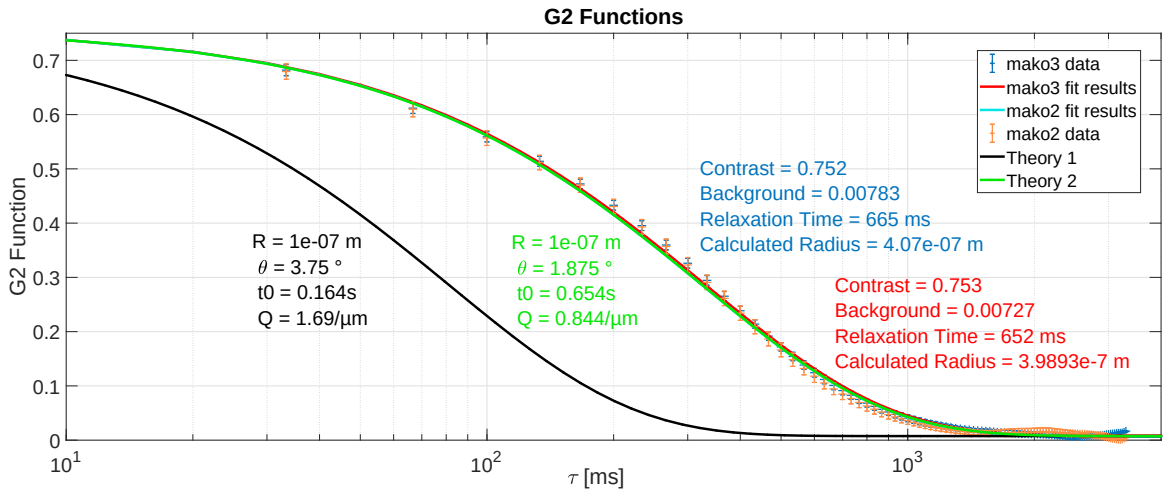

Figure 6: g_2 functions from a simultaneous symmetric measurement with both camera sensors with fitted functions and fit parameters. The black curve is a theory curve with the measured angle of the cameras, while the green theory curve shows the prediction for an angle, which is only a quarter of the measured angle to the forward beam.

References

[1] **Dynamic Light Scattering**: With Applications to Chemistry, Biology, and Physics; *Bruce J. Berne, Robert Pecora* Courier Corporation, 2013, ISBN 0486320243, 9780486320243

[2] **Correlation spectroscopy with coherent X-rays**, Gerhard Grübel, Federico Zontone, Journal of Alloys and Compounds, Volume 362, Issues 1–2, 2004, Pages 3-11, ISSN 0925-8388, DOI: 10.1016/S0925-8388(03)00555-3.

[3] **Measuring temporal speckle correlations at ultrafast x-ray sources**, C. Gutt, L. Stadler, A. Duri, T. Autenrieth, O. Leupold, Y. Chushkin, and G. Grübel, Opt. Express 17, 55-61 (2009). DOI: 10.1364/OE.17.000055

[4] **Über die von der molekularkinetischen Theorie der Wärme geforderte Bewegung von in ruhenden Flüssigkeiten suspendierten Teilchen.** Einstein, A. (1905), Ann. Phys., 322: 549-560. DOI: 10.1002/andp.19053220806